

# Dynamic- and Light-Switchable Self-Assembled Plasmonic Metafilms

Sean Cormier, Tao Ding,\* Vladimir Turek, and Jeremy J. Baumberg\*

**Large-area dynamic switchable plasmonic metafilms composed of a network of gold nanoparticles (Au NPs) and the thermo-responsive polymer poly (*N*-isopropylacrylamide) (PNIPAM) are self-assembled by casting Au@PNIPAM core-shell nanoparticles. These dense plasmonic films present an unusual optical behavior arising from the macroscale effective medium response of the film and the microscopic interactions of the gold nanoparticles. Such intensely colored plasmonic metafilms can be thermally actuated across large areas via direct heating, allowing extraction of the tuning of the effective dielectric permittivity of this metamaterial. By contrast, local plasmonic heating by illuminating the Au NPs in these metafilms enables sub-second and highly reversible contraction of the plasmonic metafilms, capable of pumping water. This work provides a paradigm for switchable metafilms and metasurfaces that can be harnessed for different applications such as sensing, imaging optics, and image displays.**

Thin-films composed of organized sub-wavelength optically resonant nanostructures produce unusual optical properties. Known as metasurfaces or metafilms, they are capable of delivering ultrathin optical components such as high-numerical-aperture lenses,<sup>[1]</sup> achromatic gratings,<sup>[2]</sup> holographic images,<sup>[3]</sup> and mode filters.<sup>[4]</sup> Typically, their fabrication utilizes lithography of high refractive index semiconductor or metallic components, producing elements operating in the near-IR spectral region. A major challenge is to create tunable versions of these metafilms, thus capable of real-time optimization and controllable performance, of tremendous utility for applications from biomedicine to displays. Although electrical gating of inorganic materials is being explored using top-down processing,<sup>[5–7]</sup> the application of metamaterials in devices operating at optical frequencies has been hindered by high losses, high dispersion, and complex lithographic fabrication with

features at subwavelength scales. The cost of such devices can be greatly reduced by exploiting the optical resonances of large-area self-assembled plasmonic nanoparticles, however their actuation has been problematic as they consist of noble metals combined with dielectrics.<sup>[8–10]</sup>

The integration of stimuli-responsive soft materials, such as polymers and liquid crystals, can bring about significant changes in size, geometry, and refractive index.<sup>[11]</sup> Since the optical properties of the interacting plasmonic particles are highly sensitive to the interparticle separation, strong color changes can be achieved by harnessing these polymers to tune the spacing between particles. Optical switching of the plasmonic systems is especially interesting because it allows for development of more complex inte-

grated plasmonic systems that can be optimized in real time. Plasmonic particles have high absorption cross-sections and thus efficiently convert irradiation into heat. Much research has thus explored combinations of plasmonic nanoparticles and temperature-responsive polymers.<sup>[12–14]</sup> In particular, there has been strong interest in using poly(*N*-isopropylacrylamide) (PNIPAM), a well-studied thermo-responsive polymer with a lower critical solution temperature (LCST) around 32 °C in aqueous solution. PNIPAM undergoes a phase transition to a hydrophobic state when the temperature is raised above the LCST, causing the polymer chains to contract. Upon cooling below the LCST, PNIPAM becomes hydrophilic and the chains extend into the water.

This PNIPAM phase transition has been used in colloidal, 2D, and 3D structures for switchable surface enhanced Raman spectroscopy (SERS) detection,<sup>[15–17]</sup> drug delivery,<sup>[18]</sup> tunable color,<sup>[19–21]</sup> and micro-actuation.<sup>[22]</sup> However almost no work has explored light-tunable plasmonic thin-films or metasurfaces consisting of gold nanoparticles (Au NPs) using this thermo-responsive actuation. A volume phase transition of gold nanorod-embedded PNIPAM hydrogel microcylinders was studied under near-infrared irradiation,<sup>[22]</sup> but showed rather slow response times  $\approx 20$  s. Other studies on Au NP-PNIPAM composite films have focused on 2D nanoparticle mats assembled at liquid-liquid interfaces,<sup>[19]</sup> and superlattices formed with  $>50$  nm thick PNIPAM shells, thicker than useful for Au NP plasmonic coupling,<sup>[21]</sup> for which light-induced actuation remains unexplored.

Here we show a simple method to form large area thermo-responsive plasmonic films which achieve the fastest switching time reported for large-area composite metafilms, and exhibit

S. Cormier, Prof. T. Ding, Dr. V. Turek, Prof. J. J. Baumberg  
NanoPhotonics Centre  
Cavendish Laboratory  
University of Cambridge  
Cambridge CB3 0HE, UK  
E-mail: t.ding@whu.edu.cn; jjb12@cam.ac.uk

Prof. T. Ding  
School of Physics and Technology  
Wuhan University  
Wuhan 430072, China

 The ORCID identification number(s) for the author(s) of this article can be found under <https://doi.org/10.1002/adom.201800208>.

DOI: 10.1002/adom.201800208

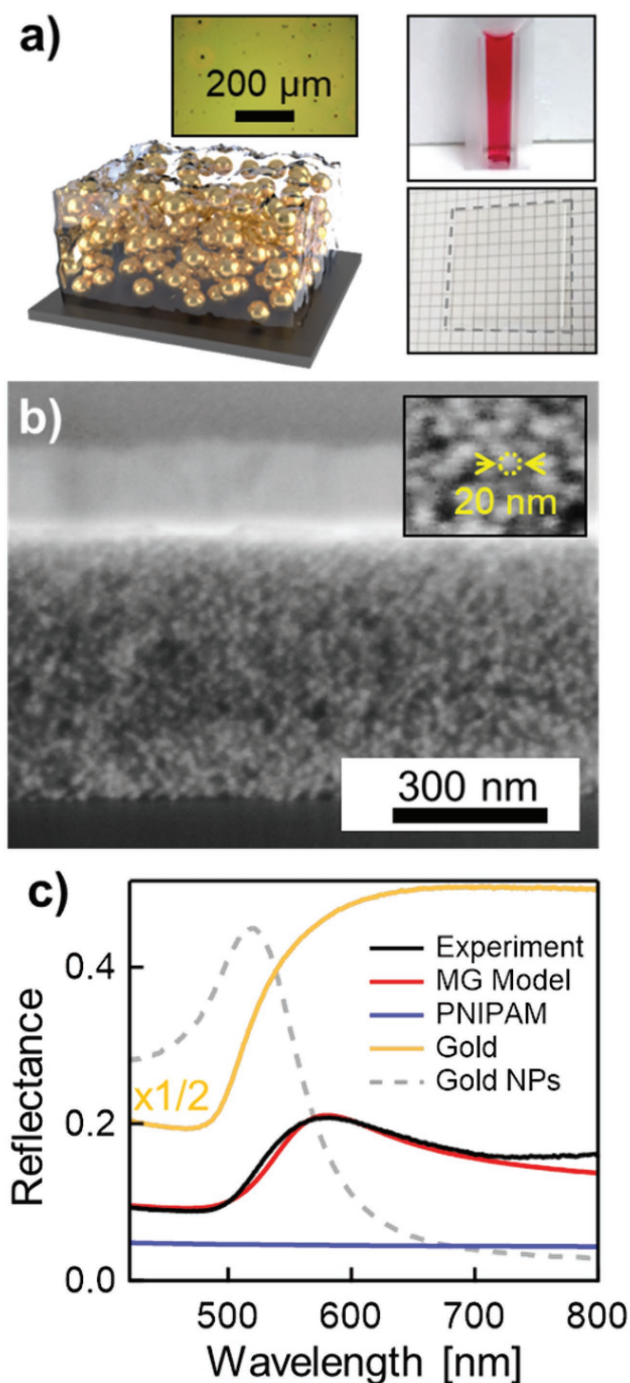


**Figure 1.** Dried Au@PNIPAM film. a) Schematic of dried Au@PNIPAM film on silicon substrate. Inset: (top-left) bright field image of Au@PNIPAM film (20× magnification, 0.45 NA), (top-right) photo of Au@PNIPAM NPs in cuvette, (bottom) photo of PNIPAM film on glass substrate without Au NPs (within dashed area, 2 mm grid). b) Scanning electron microscope (SEM) image of a thin-film cross-section milled with a focused ion beam, captured at 54° vertical tilt. Inset: Expanded SEM image of the film cross-section with a single nanoparticle circled with a dashed line. c) Reflection spectra of Au@PNIPAM (black), gold (yellow), and dry PNIPAM (blue) films, together with fitted Maxwell-Garnet (MG) effective medium model (red, see text) with  $f = 16\%$  gold fill fraction. Dashed curve is the normalized extinction curve of 16 nm Au NPs.

fully reversible dynamic color changes. Their dried optical properties are studied by casting them on silicon substrates, while deposition onto water-permeable porous membranes allows characterization of their fast switching.

We first look at the optical properties of dried Au@PNIPAM metafilms on silicon substrates (Figure 1). These are composed of randomly dispersed Au NPs in a dry non-crosslinked PNIPAM matrix (Figure 1a). The reflected color differs considerably from the color of the constituent parts. Notably, the surface appears bright green (inset Figure 1a) while the 16 nm Au@PNIPAM particles in solution are dark red and PNIPAM films are transparent. This colored reflection arises from the interface between air and an effective medium of Au NP@PNIPAM particles randomly dispersed on a scale much smaller than the wavelength of visible light, forming a metamaterial. The cross section of the dried Au@PNIPAM films (Figure 1b) clearly resolves a uniform film with densely packed Au NPs inside the PNIPAM matrix.

The reflection spectrum of the Au@PNIPAM film on a silicon substrate shows a broad peak around 580 nm, which is not easy to reconcile with any combination of spectra from PNIPAM, bulk gold, and Au NPs (Figure 1c). This peak can however be reproduced using a Maxwell-Garnett (MG) effective medium model (red line). This simplifying approximation applies to optical systems with uniform spherical inclusions randomly dispersed inside a matrix with different refractive index.<sup>[23,24]</sup> The effective permittivity of the film,  $\epsilon_{\text{eff}}$ , is determined by the permittivity of the film matrix,  $\epsilon_m$ , the interstitial particles,  $\epsilon_i$ , and relative volume fill fraction,  $f_i$ , of the particles in the film

$$\epsilon_{\text{eff}} = \epsilon_m \frac{2f_i(\epsilon_i - \epsilon_m) + \epsilon_i + 2\epsilon_m}{2\epsilon_m + \epsilon_i + f_i(\epsilon_m - \epsilon_i)} \quad (1)$$

The resulting optical properties of the Au@PNIPAM film are controlled by its thickness, gold fill fraction and PNIPAM refractive index. Our modeling (Figure 1c) shows the close packed film has  $f = 16\%$ , implying a mean Au NP@PNIPAM separation of 10.7 nm, and thus a PNIPAM coating thickness of  $\approx 5$  nm (when dry).

Reducing the gold fill fraction and total film thickness allows incident light to pass through the film and efficiently reflect back, giving rise to thin-film interference effects. A low fill-fraction Au@PNIPAM film on silicon is prepared by tripling the concentration of PNIPAM to increase the coating thickness on the Au NPs (Figure 2). Spectral line scans across the film (Figure 2a) clearly show periodic microcavity modes from the interference of light reflected from the top and bottom of the Au@PNIPAM layer. These interference bands are well fit using the Maxwell-Garnett effective medium approximation and Rouard's method for solving the optical response of thin-films (Figure 2b).<sup>[25]</sup> The gold fill fraction of the film is determined by fitting the position of the constant reflection band around 570 nm where strong absorption and scattering prevent thin-film interference effects with the MG model. Both the position and width of the reflection band depends on the gold fraction as shown in Figure 2c, giving  $f = 3.5\%$ , implying a mean Au NP@PNIPAM separation of 28 nm, and thus a PNIPAM coating thickness of  $\approx 14$  nm as expected from the modified protocol.

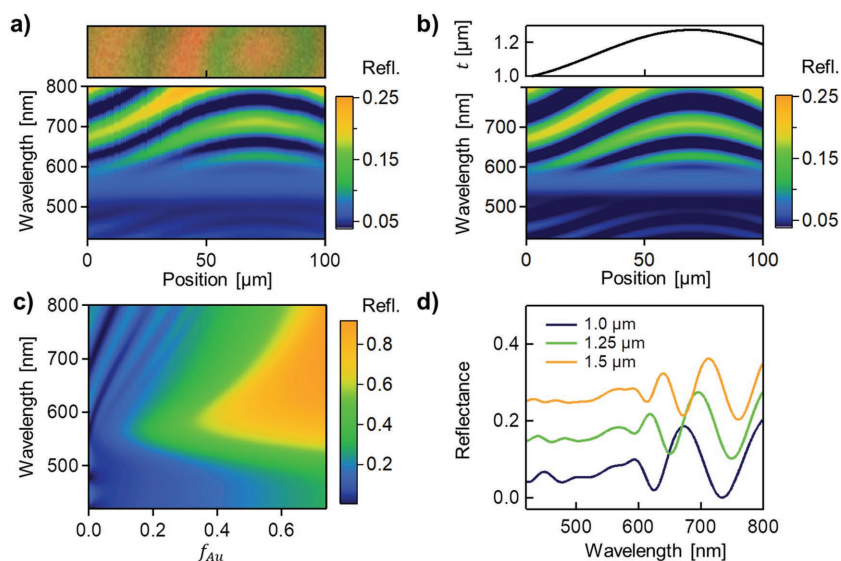


**Figure 2.** Reflectivity of low- $f_{Au}$ @PNIPAM thin-films. a) Experimental line scans of bright-field reflectivity spectra along the Au@PNIPAM film surface, image of scanned area shown above. b) Thin-film model with MG effective medium model for Au@PNIPAM film using gold fill fraction,  $f_{Au} = 3.5\%$ , and fitted thickness,  $t$ , profile shown above. c) Reflectivity model of Au@PNIPAM thin-films as a function of  $f_{Au}$  for a thickness of  $1 \mu\text{m}$ . d) Modeled reflectivity of films with  $1.0$ ,  $1.25$ , and  $1.5 \mu\text{m}$  thicknesses and  $f_{Au} = 3.5\%$ . Spectra are vertically offset.

The measurements consistently show broadened peaks which can only be modeled by introducing an additional small extinction coefficient in the polymer matrix ( $\Im m\{n\} = 0.02$ ). This correction is attributed to scattering from density fluctuations, observed directly from films of the dried polymer without Au NPs present. Increasing the thickness of the film shifts the interference modes in the spectra and decreases their separation (Figure 2d), allowing the film thickness to be precisely fit under the assumption that its refractive index remains independent of thickness. This system thus forms a 3D metallo-dielectric composite metamaterial, whose optical properties we will now show can be tuned.

PNIPAM exhibits temperature-induced volume changes only in aqueous solution. The Au@PNIPAM films are thus deposited on porous aluminum oxide membranes that are water permeable but impermeable to the nanoparticles (Figure 3). The membranes are then placed on top of a water reservoir, ensuring the top surface of the sample is not covered by water, in order to prevent dissolution of the non-crosslinked Au@PNIPAM films. Cycling the temperature of the water reservoir above and below the LCST of PNIPAM, correspondingly expels and absorbs water out of/into the Au@PNIPAM film from the reservoir below (Figure 3a). This swelling and shrinking of the films give a strong optical response. Thin-film interference is not observed for these films as the underlying

aluminum oxide membrane is highly optically diffusive. The change in color of the films is thus a result of changing the interparticle distance of the plasmonic Au NPs. Upon heating the water reservoir, the peak reflectivity red shifts from  $570$  to  $600 \text{ nm}$  and the scattering strength doubles (Figure 3b) as the PNIPAM collapses, reducing the Au NP separation thus strengthening the coupling between the Au NPs, as well as increasing the refractive index of the PNIPAM matrix from  $1.33$  to  $1.42$ .<sup>[26]</sup> In addition to the strong color change, the film also undergoes a change in reflection amplitude due to the increase in effective refractive index of the composite film upon heating. This thermal-induced color change of the plasmonic metamaterials is reproducible (Figure 3c) as seen by tracking the resonance peak over several heating and cooling cycles.

These experiments thus allow the effective refractive indices and gold fill fractions to be extracted for metamaterials in expanded and collapsed states. The MG model is used to fit the observed reflectance and extract information on the composition of the films. The peak

positions and shapes fit well (Figure 3b), but do not capture the tails of increased reflectance attributed to additional scattering from the porous aluminum oxide membrane. The model implies that the fill fraction of gold is significantly higher when the film is wet, although the reflected intensity peak is smaller

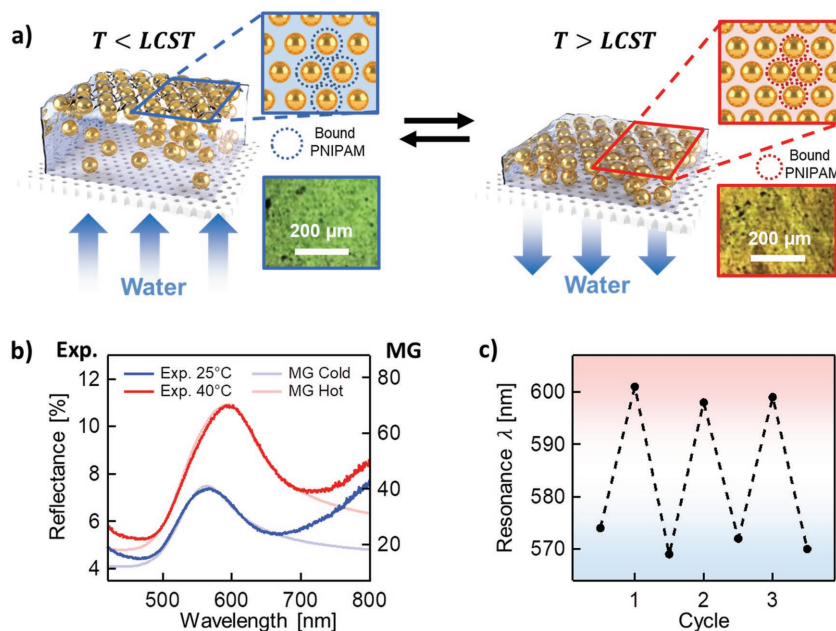


**Figure 3.** Temperature response of Au@PNIPAM films on porous anodized aluminum membranes. a) Schematic of Au@PNIPAM film actuation in response to temperature cycling, corresponding microscope images to lower-right ( $5\times$  magnification,  $0.15 \text{ NA}$ ). b) Reflection spectra of Au@PNIPAM film above and below the LCST, with MG fits plus background scattering contributions. c) Peak resonance shifts over several temperature cycles from  $25$  to  $40 \text{ }^\circ\text{C}$ .

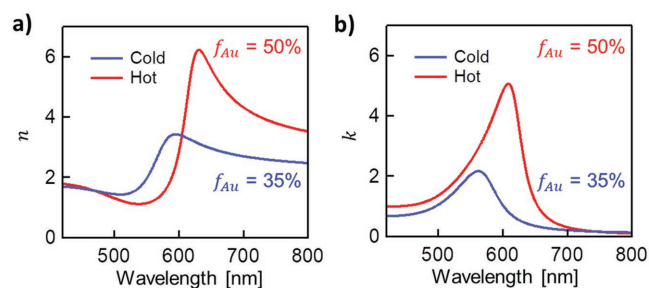


**Figure 4.** Maxwell-Garnett model of effective metafilm complex refractive index. Extracted effective a) real and b) imaginary parts of refractive index at temperatures above (hot) and below (cold) the LCST of 32 °C.

than expected from the model (likely due to diffusive scattering losses from the rough substrate). The gold fill fractions are  $\approx 35\%$  for the swollen state and  $\approx 50\%$  for the collapsed state, suggesting Au NP mean separations of 4.5 and 2.2 nm. Accounting for these results suggests that a very dense, nearly close-packed layer of Au NPs accumulates at the air-film interface and dominates the reflectance of the wetted films. Using these MG model results, provides the effective complex refractive index of the switchable metafilms in the swollen (cold) and contracted (hot) states (Figure 4). Both real and imaginary parts roughly double, with  $n > 6$  on resonance in the hot collapsed state. We however note that at the high fill fractions in this top layer, the MG formalism is less reliable, but analytic models are not yet available for such random metafilm organization.

The color change in response to global heating is relatively slow due to the time required to heat and passively cool the entire water reservoir below the film. In order to improve the switching speed of the films, plasmonic heating is used. Cycling the 447 nm laser irradiation causes the film to rapidly collapse and swell. Light-induced heating occurs locally at the beam spot without heating the water reservoir, reducing the switching time from minutes to milliseconds compared to global heating. Here we define the switching time as the time elapsed between 10 and 90% of the full optical changes either from the swollen state to the collapsed state or vice versa. The metafilm now acts as a light-driven water pump, expelling the water on heating above the LCST via the enhanced optical cross section of the Au NP metafilm, and sucking back in the water on cooling.

The transition of the film is clearly observed with laser power (Figure 5). Due to the large absorption cross-section of these dense nanoparticle films, powers densities as low as  $0.5 \text{ W cm}^{-2}$  induce resonance shifts  $>20 \text{ nm}$  and double the reflectivity in the red (Figure 5a). The switching of the peak reflection during cycling is highly robust. We see full recovery of the films after irradiation (Figure S1, Supporting Information). Six cycles of laser switching every 30 s demonstrate this reproducible shifting of peak reflectivity (Figure 5b), from  $554 \pm 1 \text{ nm}$  (dark) to  $585 \pm 3 \text{ nm}$ . The redshift timescale after switching on the laser is sub-second, while the recovery of the film when the laser

is switched off is slower (of order seconds). The discrepancy between the rates of contraction and recovery can be understood in terms of the molecular kinetics of water expulsion from the swollen PNIPAM matrix and its re-absorption back into the contracted PNIPAM matrix. Large pores in the swollen PNIPAM matrix allow water to quickly escape the matrix as the metafilm contracts, whereas the smaller pores in the collapsed PNIPAM matrix limit the rate of re-absorption during swelling. This suggests that further tuning of the pore microstructure of these composite films can further enhance their switching speeds.

In summary, we demonstrate the ability to dynamically tune the reflectance of simply-deposited plasmonic metafilms by both direct heating and light-induced heating. Combining the coil-to-globule temperature response of PNIPAM with the plasmonic properties of Au NPs, we show the dynamic thin-film coloration of the composite metallo-dielectric metamaterial. Direct heating of the film results in complete actuation of the films, whereas light-induced heating enables local control of the film actuation. Furthermore, we demonstrate that porous membranes such as aluminum oxide can enable the wetting and de-wetting of such polymer-plasmonic particle composite films. This avoids complicated crosslinking of the gel and enables large swelling ratios and faster switching rates. The resulting changes in surface topography, roughness, and color exhibited by these metafilms can be harnessed for applications such as large-scale tunable colored wallpapers and coatings, and real-time switchable patterned surfaces such as for bioscaffolds or metalenses. In addition, such films hold significant potential for a variety of functional applications, such as temperature sensors, local wetting transformations, and for tunable SERS sensors.

## Experimental Section

**Au@PNIPAM Particle Synthesis:** Au@PNIPAM particles were prepared via the ligand exchange method. The 16 nm Au NPs were synthesized using Turkevich's method.<sup>[27,28]</sup> Briefly, an  $86 \text{ mg L}^{-1}$  aqueous solution of gold(III) chloride trihydrate ( $\geq 99.9\%$  trace metal basis, Sigma Aldrich) was stirred and heated to steady-state reflux conditions and then  $200 \text{ mg L}^{-1}$  of trisodium citrate dehydrate was added quickly. The trisodium

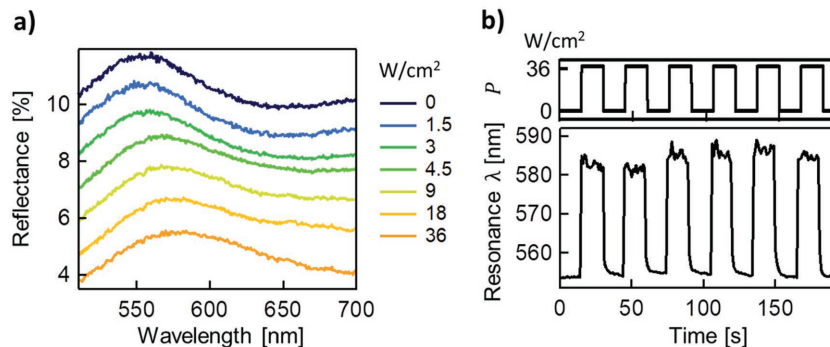


**Figure 5.** Light-induced actuation of the Au@PNIPAM films on porous anodized aluminum membranes. a) Power dependence of Au@PNIPAM film reflectivity spectra under increasing 447 nm irradiation (spectra offset for clarity). b) Resonance peak wavelength shift metafilm reflection spectra over seven irradiation cycles at  $P = 36 \text{ W cm}^{-2}$  with 447 nm light focused to a  $42 \mu\text{m}$  diameter spot.

citrate dehydrate reduced and stabilized the Au NPs at a diameter of  $16 \pm 2$  nm, confirmed by dynamic light scattering (Malvern ZetaSizer) and electron microscopy (Zeiss LEO 1530VP). The citrate-capping of the Au NPs was exchanged with PNIPAM by adding  $20 \times 10^{-6}$  M of 5.5 kDa  $\text{NH}_2$ -terminated PNIPAM (Sigma-Aldrich) while heating at  $40^\circ\text{C}$ . The successful ligand exchange was clearly identified by the heat-induced reversible color-change of the Au@PNIPAM particle solution from red to violet as reported in detail elsewhere.<sup>[29]</sup>

**Film Preparation:** The Au@PNIPAM films were prepared by highly concentrating the Au@PNIPAM particle solution using two centrifugation steps and then casting. The synthesized Au@PNIPAM particle solution was spun at 14 500 rpm in a microcentrifuge (Eppendorf miniSpin) for 10 min and the supernatant was decanted. Chloroform was added to the centrifuge tube, which was immiscible with the aqueous Au@PNIPAM particle solution. A subsequent centrifugation at 14 500 rpm for 10 min forced the Au@PNIPAM particles into the chloroform phase. After decanting the aqueous phase, the chloroform phase was dried. The resulting dried Au@PNIPAM particles were re-dispersed in chloroform for casting on silicon wafers and aluminum oxide membranes (Whatman Anodisc,  $0.02 \mu\text{m}$  pore size).

**Characterization:** The dried structure of the Au@PNIPAM films was characterized with electron microscopy. Focused ion beams were used to mill wedge structures in the films for cross-sectional electron imaging. Prior to imaging, the films were coated with 100 nm of gold by e-beam evaporation and in situ 80 nm of platinum by ion-beam-induced gas deposition. The gold layer served to reduce charging during imaging and the platinum improved the perpendicularity of the cross-section. The milling and imaging were both performed in an FEI Helios NanoLab instrument.

The reflectivity of the films was measured with a customized Olympus BX51 microscope equipped with a  $50 \mu\text{m}$  fiber-coupled QE65000 Ocean Optics spectrometer, a single-mode fiber-coupled 447 nm continuous wave laser, and a Prior translation stage, which were automated. This laser wavelength can be conveniently filtered out to allow real-time monitoring of the local film reflectivity at longer wavelengths. The temperatures of the films deposited on aluminum oxide membranes were precisely regulated by heating the water below the samples with a hot stage (TMS 92, Linkam). For studying the light-induced response of the films, the laser power was electronically controlled and calibrated. A  $\lambda > 500$  nm long pass filter was used to remove the scattered laser from the light collected by the spectrometer.

## Supporting Information

Supporting Information is available from the Wiley Online Library or from the author.

## Acknowledgements

J.J.B. and T.D. conceived the idea, S.C. fabricated and characterized the films. All authors contributed to the discussion, analysis, and writing up of this work. This research was supported by UK Engineering and Physical Sciences Research Council grants EP/G060649/1 and EP/L027151/1, ERC grant LINASS 320503, and Leverhulme Trust (ECF2016-606). The authors acknowledge the Cavendish Laboratory Electron Microscopy Suite for their support and expertise. T.D. thanks the support of start-up grant from Wuhan University and 1000-talents Programme (Youth) from Chinese government. S.C. is grateful for the support from the Winton Programme for the Physics of Sustainability.

## Conflict of Interest

The authors declare no conflict of interest.

## Keywords

composite metallo-dielectric, gold, metafilms, metamaterials, poly(*N*-isopropylacrylamide)

Received: February 15, 2018

Published online:

- [1] X. Zhang, Z. Liu, *Nat. Mater.* **2008**, *7*, 435.
- [2] M. Khorasaninejad, F. Capasso, *Nano Lett.* **2015**, *15*, 6709.
- [3] X. Li, L. Chen, Y. Li, X. Zhang, M. Pu, Z. Zhao, X. Ma, Y. Wang, M. Hong, X. Luo, *Sci. Adv.* **2016**, *2*, 11.
- [4] V. A. Fedotov, J. Wallauer, M. Walther, M. Perino, N. Papisimakis, N. I. Zheludev, *Light. Sci. Appl.* **2015**, *4*, 306.
- [5] J. Lee, S. Jung, P.-Y. Chen, F. Lu, F. Demmerle, G. Boehm, M.-C. Amann, A. Alù, M. A. Belkin, *Adv. Opt. Mater.* **2014**, *2*, 1057.
- [6] Y.-W. Huang, H. W. H. Lee, R. Sokhoyan, R. A. Pala, K. Thyagarajan, S. Han, D. P. Tsai, H. A. Atwater, *Nano Lett.* **2016**, *16*, 5319.
- [7] S. Kim, M. S. Jang, V. W. Brar, Y. Tolstova, K. W. Mauser, H. A. Atwater, *Nat. Commun.* **2016**, *7*, 12323.
- [8] F. Huang, S. Drakeley, M. G. Millyard, A. Murphy, R. White, E. Spigone, J. Kivioja, J. J. Baumberg, *Adv. Opt. Mater.* **2016**, *4*, 328.
- [9] K. J. Si, D. Sikdar, Y. Chen, F. Eftekhari, Z. Xu, Y. Tang, W. Xiong, P. Guo, S. Zhang, Y. Lu, Q. Bao, W. Zhu, M. Premaratne, W. Cheng, *ACS Nano* **2014**, *8*, 11086.
- [10] J. B. Edel, A. A. Kornyshev, A. R. Kucernak, M. Urbakh, *Chem. Soc. Rev.* **2016**, *45*, 1581.
- [11] I. Tokarev, S. Minko, *Soft Mater.* **2009**, *5*, 511.
- [12] I. Tokarev, S. Minko, *Soft Mater.* **2012**, *8*, 5980.
- [13] M. Nguyen, N. Felidj, C. Mangeney, *Chem. Mater.* **2016**, *28*, 3564.
- [14] W. Lewandowski, M. Fruhnert, J. Mieczkowski, C. Rockstuhl, E. Górecka, *Nat. Commun.* **2015**, *6*, 6590.
- [15] M. Nguyen, A. Kanaev, X. Sun, E. Lacaze, S. Lau-Truong, A. Lamouri, J. Aubard, N. Felidj, C. Mangeney, *Langmuir* **2015**, *31*, 12830.
- [16] R. Contreras-Cáceres, J. Pacifico, I. Pastoriza-Santos, J. Pérez-Juste, A. Fernández-Barbero, L. M. Liz-Marzán, *Adv. Funct. Mater.* **2009**, *19*, 3070.
- [17] H. Gehan, L. Fillaud, M. M. Chehimi, J. Aubard, A. Hohenau, N. Felidj, C. Mangeney, *ACS Nano* **2010**, *4*, 6491.
- [18] M. Nguyen, X. Sun, E. Lacaze, P. M. Winkler, A. Hohenau, J. R. Krenn, C. Bourdillon, A. Lamouri, J. Grand, G. Lévi, L. Boubekeur-Lecaque, C. Mangeney, N. Félidj, *ACS Photonics* **2015**, *2*, 1199.
- [19] T. Ding, A. W. Rudrum, L. O. Herrmann, V. Turek, J. J. Baumberg, *Nanoscale* **2016**, *8*, 15864.
- [20] T. Ding, C. Rüttiger, X. Zheng, F. Benz, H. Ohadi, G. A. E. Vandenbosch, V. V. Moshchalkov, M. Gallei, J. J. Baumberg, *Adv. Opt. Mater.* **2016**, *4*, 877.
- [21] M. Karg, T. Hellweg, P. Mulvaney, *Adv. Funct. Mater.* **2011**, *21*, 4668.
- [22] A. Shiotani, T. Mori, T. Niidome, Y. Niidome, Y. Katayama, *Langmuir* **2007**, *23*, 4012.
- [23] J. C. M. Garnett, *Philos. Trans. R. Soc., A* **1904**, *203*, 385.
- [24] O. Zhuromsky, *Crystals* **2017**, *7*, 1.
- [25] P. Lecaruyer, E. Maillart, M. Canva, J. Rolland, *Appl. Opt.* **2006**, *45*, 8419.
- [26] B. W. Garner, T. Cai, S. Ghosh, Z. Hu, A. Neogi, *Appl. Phys. Express* **2009**, *2*, 057001.
- [27] J. Kimling, M. Maier, B. Okenve, V. Kotaidis, H. Ballot, A. Plech, *J. Phys. Chem. B* **2006**, *110*, 15700.
- [28] J. Turkevich, P. C. Stevenson, J. Hillier, *J. Phys. Chem.* **1953**, *57*, 670.
- [29] T. Ding, V. K. Valev, A. R. Salmon, C. J. Forman, S. K. Smoukov, O. A. Scherman, D. Frenkel, J. J. Baumberg, *Proc. Natl. Acad. Sci. USA* **2016**, *113*, 5503.